Int. J. Electrochem. Sci., 17 **(2022)** Article Number: 221139, doi: 10.20964/2022.11.43

International Journal of
ELECTROCHEMICAL
SCIENCE
www.electrochemsci.org

Kinetic Analysis of the X100 Steel Corrosion in Brine containing Inhibitor (Imidazoline) under different Turbulent Flow Conditions

Clarisa Campechano-Lira[1], *ArnoldoBedolla-Jacuinde*[2], *Andres Carmona- Hernández*[3], *Ricardo Orozco-Cruz*[3], *Araceli Espinoza-Vazquez*[3], *Ricardo Galvan-Martinez*[3,*]

[1] Centro MICRONA, Universidad Veracruzana, Adolfo Ruiz Cortines No 455, Fracc. Costa Verde, Boca del Río, Veracruz, C.P. 94294, México.
[2] Instituto de Investigación en Metalurgia y Materiales, Universidad Michoacana de San Nicolás de Hidalgo. Ciudad Universitaria, C.P. 58030-Morelia, Michoacán, México
[3] Unidad Anticorrosión-Instituto de Ingeniería, Región Veracruz, Universidad Veracruzana, Av. Juan Pablo II, Zona Universitaria, Boca del Río, Veracruz, C.P. 94294, México.
[*]E-mail: rigalvan@uv.mx

Received: 17 August 2022 / *Accepted:* 16 September 2022 / *Published:* 10 October 2022

The accidents produced by the effects of corrosion on the pipeline steels used in the oil industry to transport the hydrocarbons and its derivatives, can be generating human and economic loss. This paper presents a study of the anodic and cathodic kinetics of an API X100 steel by the potentiodynamic polarization curves under turbulent flow conditions. The X100 steel was immersed in a NACE brine with 50 ppm of corrosion inhibitor dissolved under turbulent flow conditions at room temperature and atmospheric pressure of the Veracruz Port. In order to simulate the hydrodynamic conditions, a Rotating Cylinder Electrode (RCE) with different rotation speed was used. Electroactive species to be reduced were determined using the Eisenberg equation, as well as an analysis with dimensionless numbers was made to complement the study. Anodic kinetic analysis shown that the i_{corr} was flow dependent and the values of anodic Tafel slopes were typical to activational or charge transfer corrosion process. On the other hand, the analysis of cathodic kinetics shown that the system under turbulent flow conditions is dominated by the oxygen diffusion (mass transfer process) from the bulk to metallic surface. According to the comparison of the experimental cathodic current and the theoretical limiting current attained by the Eisenberg equation, it can be established that the cathodic kinetics of the process is dominated by an oxygen reduction reaction.

Keywords: RCE, dimensionless numbers, Eisenberg equation, Turbulent Flow, corrosion inhibitor

1. INTRODUCTION

According with the technological and research advances, many researchers have developed different steel types with better properties, such as high mechanical resistance, toughness, and weldability through the microstructural modification with low quantities of microalloyings like niobium (Nb), vanadium (V) and titanium (Ti), and with a controlled thermomechanical treatment. [1-5] The metals with these characteristics are the steel with high resistance and low alloy (HSLA) that later were called microalloying steels and they are revolutionizing the automotriz, oil and gas industries. In this context, the HSLA steels are widely used in the pipeline that transport hydrocarbons and its derivatives, where some aggressive factors are presented, such as fatigue, high pressure, and turbulent flow conditions. [6-11] One example of the HSLA steel is the API X100, this steel shows high mechanical resistance, tenacity, and weldability. In recent years, this X100 steel have been used in the Antarctic and Subarctic zones where the pipeline experience high internal pressure and severe experimental conditions. [10,12-14] According the properties of this steel, it has showed to be a good candidate to use in tools and machinery sectors, in the aerospace and military industry, in the oil industry, mainly in the pipelines that transport hydrocarbons, [15,16] however, it needs to prove to be better that the conventional steels through mechanical assays, wear, and corrosion test. It is because the pipelines steel is under fatigue, wear, stress, and corrosive environments. [17]

The metals corrosion resistance is a factor related with the corrosion products film adsorbed on metallic surface, and in turn, this film can define the corrosion morphology and determinate de corrosion kinetic. [18] The corrosion process in an aerated environment is attributed to two parameters, the dissolved oxygen and mainly to the ions chloride (Cl^-) concentration because these ions chloride can affect the anodic dissolution of the Fe by the adsorption process between the Cl^- and the OH^- causing the decrease in the charge transfer resistance. [19,20] According to these parameters, it is possible to note that the corrosion process can be analyzed individually, studying the effects of the anodic and cathodic reaction on corrosion Speed (CR) by the electrochemical corrosion technique. Some researchers like Lara-Banda and Montoya-Rangel [5, 21, 22] have studied the metals and alloys by electrochemical techniques, such as electrochemical impedance spectroscopy (EIS), electrochemical noise (EN), and polarization curves (PC). In order to analyze the corrosion reaction by separated, the polarization curves are a great tool because, with these PC are possible to sweep in both directions (anodic and cathodic zones) as a function of the corrosion potential (E_{corr}) and calculate the corrosion speed. [23,24]

The X100 steel can be used as pipeline in the hydrocarbons transport and this steel in the internal corrosion of the pipeline can suffer the flow accelerated corrosion (FAC), where this FAC is different from erosion, it is an electrochemical process assisted by mass transfer and chemical dissolution. FAC is the main cause of the pipelines' failures due to the thickness reduction in metals. The corrosion products function as a protective film on the metal surface slowing down the corrosion speed. However, due to the hydrodynamic conditions, these products dissolve, thus decreasing the thickness of the film of corrosion products adsorbed on the metal surface, becoming thinner and less protective. The film can be broken or completely removed and leave the metal surface exposed. [25,26]

In order to study the FAC, several hydrodynamic studies to simulate turbulent flows have been proposed. However, the approaches based on the analysis of kinetics and mass transportation using the

Rotating Cylinder Electrode (RCE) at different rotation speeds show important advantages when compared with other methods, ones of the most important advantages are that at little Reynolds number (Re) is possible to get the turbulent flow conditions, at Re 200 approximately. Turbulent conditions in corrosion comprise the metal dissolution, oxygen reduction, and stability of surface oxide films. [27,28]

It is important to point out that another study of the corrosion under turbulent flow conditions are the dimensionless number analysis and the correlations of dimensionless numbers have been introduced to corrosion studies because they provide expressions that allow to characterize the fluid based on the flow conditions. Some dimensionless numbers used to these studies are Schmidt, Sherwood, and Reynolds. [29-32]

Schmidt number (Sc) is associated to mass transfer properties into fluid and Sherwood number (Sh) to mass transfer coefficient (ki) of a given species in a fluid. Flow regimes may be classified according to the Reynolds number (Re) as laminar or turbulent. [33] The critical Reynolds number for RCE is 200, [34-38] in which transition between regimens come on.

One important point in the behavior of the corrosion phenomenon are the inhibitors. Many compounds are used in the industry, but one of the most important inhibitors are the film formers like to the imidazoline. This imidazoline can be oil-soluble and insoluble in water or oil-soluble and dispersible in water. [39,40]

This work presents the results of X100 steel immersed in NACE brine at different hydrodynamic conditions using an inhibitor as chemical metals protector and the anodic - cathodic analysis to obtain the effects of the turbulent flow conditions on the corrosion phenomenon.

2. MATERIALS AND METHODS

2.1 Electrochemical Characterization

2.1.1 Working electrode.

The working electrodes used during the electrochemical study were made of a segment of grade X100 steel. This steel segment was sectioned in cylinders with a dimension of 0.011 m height and 0.012 m of diameter with a total exposed area of 0.000415 m^2. These metallic cylinders were sanded with a 220 to 600 grit SiC paper. Then, the cylinders were rinsed with distilled water and hot air dry. The chemical composition of the X100 steel is presented in Table 1.

Table 1. Chemical composition of X100 steel (wt.%).

Element	Fe	C	Mn	Si	Cu	Ni	Cr	Mo	Nb	V	Ti
Wt. %	**96.39**	**0.05**	**1.75**	**0.36**	**0.51**	**0.29**	**0.36**	**0.19**	**0.03**	**0.03**	**0.04**

2.2 2. Electrochemical Array.

Flow conditions were simulated using the Rotating Cylinder Electrode (RCE). Additionally, the electrochemical cell consisted of a three-electrode arrangement, it is, an X100 steel cylinder as a working

electrode, a Saturated Calomel Electrode (SCE) as a reference electrode, and a platinum bar as auxiliary electrode.

The electrolyte used in this experiment is a NACE 1D182 [41] brine containing 50 ppm of a corrosion inhibitor (a commercial imidazoline). [39,40,42] NACE brine has the following chemical composition: 96.2 g/L NaCl, 3.05 g/L $CaCl_2$ and 1.86 g/L $MgCl_2$. The polarization range used for the cathodic polarization curves (CPC) was from -0.500 to +0.050 V vs E_{corr}, with a potential scan speed of 0.001 V/s. On the other hand, to anodic polarization curve (APC) was from -0.050 to 0.500 V vs E_{corr}, with a potential scan speed of 0.001 V/s. Finally, the rotating speeds (RS) of 100, 1000, 2000, 3000, 4000, 5000 and 6000 rpm were used to simulate the hydrodynamic conditions. The experiments were carried out at room temperature and atmospheric pressure of the Veracruz Port. It is important to point out that in the cathodic kinetics analysis, the Eisenberg equation, as well as dimensionless numbers like Sherwood and Schmidt, were considered. In addition, Tafel extrapolation method was used to obtain the corrosion current density (i_{corr}) in the anodic curves.

3. RESULTS AND DISCUSSION

3.1 Correlation between the rotation and Peripheral speed of the electrode and the Reynolds number.

Reynolds number is a dimensionless number dependent on the fluid velocity or the electrode rotation speed according to the density and viscosity of the fluid. It is a characteristic dimension in order to define the type of flow. [43] The Reynolds number for a RCE is given by the following expression:

$$Re = \frac{U_{RCE}\, d_{RCE}}{\nu} = \frac{U_{RCE}\, d_{RCE}\ \rho}{\mu} = \qquad (2)$$

Where ρ and μ is the density and viscosity of the environment, respectively. It is clear from this equation that there is a linear relationship between the Reynolds number (Re) and the rotation speed of the electrode. Figure 1 shows all rotational speed (rpm) expressed as peripheral speed (m/s) its correlation with the Reynolds number.

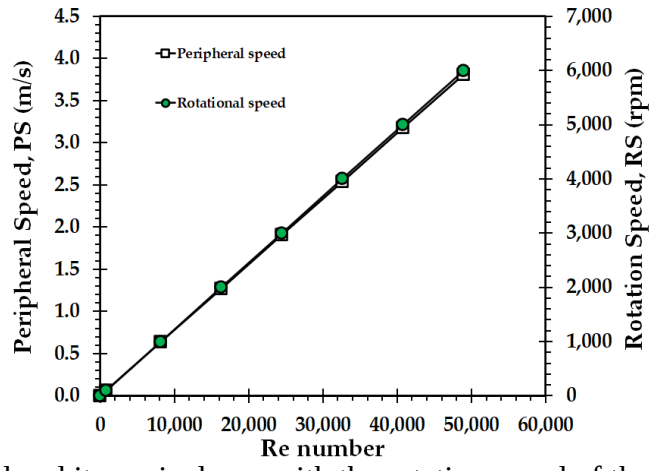

Figure 1. Peripheral speed and its equivalence with the rotation speed of the working electrode and the calculated Reynolds number.

The curve corresponding to RS vs Re is shown in Figure 1, the increment of the rotational speed (or peripheral speed) is directly proportional to the increment of the Re number.

3.2 Corrosion potential (E_{corr}) vs Reynolds number (Re).

Figure 2 shows E_{corr} results as a function of the Re number obtained from measurements of API X100 steel immersed in NACE brine under static (0 rpm) and turbulent flow conditions (100, 1000, 2000, 3000, 4000, 5000 and 6000 rpm) with and without corrosion inhibitor at room temperature and atmospheric pressure of the Veracruz Port. The curve corresponds to potential without inhibitor show that after the Re number of 8157.83 (1000 rpm) the E_{corr} values got a stable value with a potential difference of 0.005 V approximately. In case of curve corresponding to potential with 50 ppm of corrosion inhibitor, the E_{corr} values increased to get a stable behavior after a number Re of 32631.33 (4000 rpm) with a potential difference at the end of the experiment of 0.007 V.

E_{corr} results obtained by Barmatov [44] about the inhibition efficiency of propargyl alcohol on AISI 1018 mild carbon steel immersed in 4 M hydrochloric acid presented a similar behavior. It is important to point out that at Re number of 24473.5 (3000 rpm), the E_{corr} had a more electronegative value, with a difference of 0.035 V approximately, [45] attributing this behavior to the fact that at these RS there is a transition into the turbulent flow regions. This phenomenon is since this regime can present two regions, the first at the start zone of the turbulent regime and the second zone with the complete turbulence. [46,47] The E_{corr} values of the X100 steel in NACE brine registered increments are approximately ± 0.030 V.

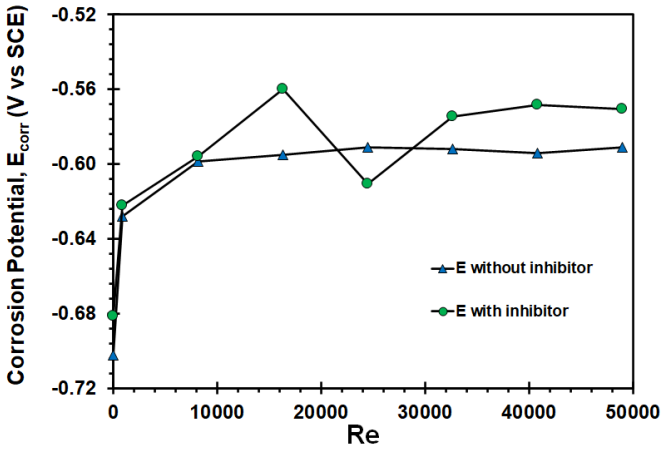

Figure 2. Corrosion potential (E_{corr}) of the X100 steel immersed in NACE brine with and without inhibitor as a function of the Re

It is important to point out that in case of the E_{corr} of the X100 steel immersed in NACE brine without corrosion inhibitor, at 100 rpm, the E_{corr} increased towards electropositive values, and it got its

stabilization at 2000 rpm. While the E_{corr} of the X100 steel immersed in the electrolyte with 50 ppm of corrosion inhibitor got the stabilization at 4000 rpm.

3.3 Analysis of anodic reaction

Figure 3 shows the anodic polarization curves (APC) obtained on API X100 cylindrical steel electrodes immersed in the NACE brine without (3a) and with (3b) corrosion inhibitor, at room temperature and atmospheric pressure, for different rotation speeds. Figure 3a shows the APC of the X100 steel in NACE brine without inhibitor. In this figure, it is possible to observe that the anodic Tafel slopes (ba) are low (between 0.100 and 0.120 V). This observation suggests that an activational process taking place on surface of the electrode. According to this fact, it is possible to point out that the anodic reaction is limited by a charger transfer process. On the other hand, the APC observed in Figure 3b shows a similar behavior to the APC shown in figure 3a, where a charge transfer process limited the anodic reaction. Figure 4 shows the calculated anodic Tafel slopes corresponding to the APC of the figure 3.

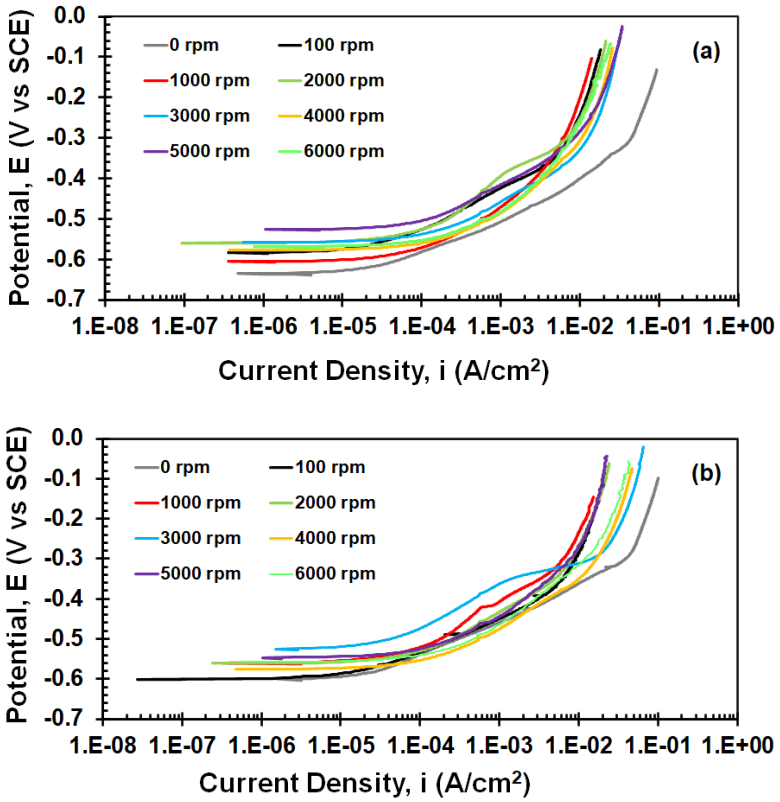

Figure 3. Anodic polarization curves of X100 steel immersed in NACE brine at different rotation speed without (a) and with (b) corrosion inhibitor.

Figure 4 shows that the anodic slopes have values located in the Tafel zone that they correspond to a corrosion process limited by the activational or charge transfer process.

According to the Tafel slopes showed in figure 4, the process observed in the anodic reaction for the two conditions (steel corrosion in seawater and seawater plus inhibitor) is the activational or charge transfer process and it is important to point out that the turbulent flow conditions have no influence on the anodic Tafel slopes, but the activational process is flowed dependent, because the corrosion current density (i_{corr}) values increased as the RS also increased. These observations indicate that anodic kinetics of the X100 steel under turbulent flow is flowed independently to the anodic Tafel slopes, but with respect to the corrosion process, it can be associated to the increment of the charge transfer phenomena. [48]

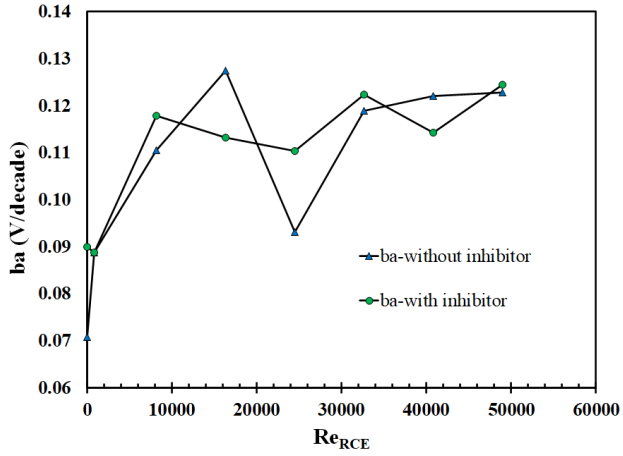

Figure 4. Calculated anodic Tafel slopes as a function of Reynolds number. X100 cylindrical steel electrode immersed in NaCl brine with and without inhibitor at different rotation speed.

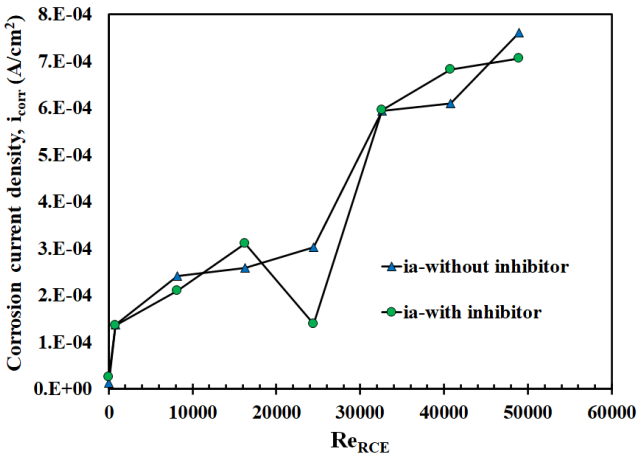

Figure 5. Measured corrosion current density of the X100 steel immersed in NACE brine with and without corrosion inhibitor as a function of the Re.

In figure 5 is possible to observe that the curve corresponding to steel corrosion immersed in brine without inhibitor, as the Re number increased, the values of i_{corr} also increased. This behavior is

attributed to the fact that as the rotation speed increased, the effect of the turbulent flow on the metallic surface also increased. It is because the flow that hit the corrosion products film adsorbed on metallic surface, and it can provoke the rupture of this film and generate more active surface increasing the i_{corr}. On the other hand, the i_{corr} curve corresponding to the steel corrosion with inhibitor, the behavior of the i_{corr} values is similar to the i_{corr} behavior of the steel corrosion without inhibitor, except to the i_{corr} at 3000 rpm.

3.4 Analysis of cathodic reaction

Figure 6 shows the cathodic polarization curves of the X100 steel immersed in NACE brine with and without 50 ppm of corrosion inhibitor at different rotation speeds: 0 (static condition), 100, 1000, 2000, 3000, 4000, 5000 and 6000 rpm.

In Figure 6a, at 0 rpm is possible to observe a typical Tafel slope corresponding to a charge-transference process, but when the medium reaches the turbulent flow conditions (as the rotation speed increases) the corrosion phenomenon is affected by a mass transfer process and a not well defined Tafel slopes are observed, it is, a diffusional process is affected the corrosion behavior. [49] This behavior is reflected through the change in the Tafel slopes with the formation of a limiting current density ($i_{lim,i}$) which indicates that there exists a larger transfer of the cathodic reagent, mainly the O_2 transfer from the bulk of the solution toward to metallic surface.

Barik [50] shows similar results with the cathodic potentiodynamic curves obtained by the electrodes of copper and nickel-aluminum by wall-jet immersed in 3.5 wt.% NaCl solution. It is important to point out that after 100 rpm, the Tafel slopes shown a typical $i_{lim,i}$ indicating a characteristic mass transfer process. In addition, [50,51] in their studies shown results about that the potentiodynamic polarization curves have three different zones, charge transfer, mixed zone and mass transport controlled (diffusion limited). According to Barik studies and taking the charge transfer zone, the corrosion current density (i_{corr}) was obtained in all anodic polarization curves and, these i_{corr} were acquired using Tafel extrapolation method. [51,52]

Barmatov [53] in his research shown that the shear stress generated between the fluid movement and the metallic surface could provoke the erosion of the inhibitor layer plus the corrosion products film (films absorbed) and rupture or elimination of these films incrementing the limiting current density, and consequently, the corrosion speed. This behavior is better observed from 1000 rpm, where the $i_{lim,i}$ increased. However, it is important to point out that the variations that exists between the rotation speeds from 1000 to 6000 rpm are small.

Figure 6b shows the cathodic curves of the steel immersed in NACE brine with 50 ppm of corrosion inhibitor. This figure shown that under static conditions (0 rpm) a behavior influenced by mass transfer through the film adsorbed on surface metallic is presented. This behavior is attributed to the presence of the different products formed from the corrosion inhibitor, which are adsorbed on the metallic surface and limits the charge transfer. [54]

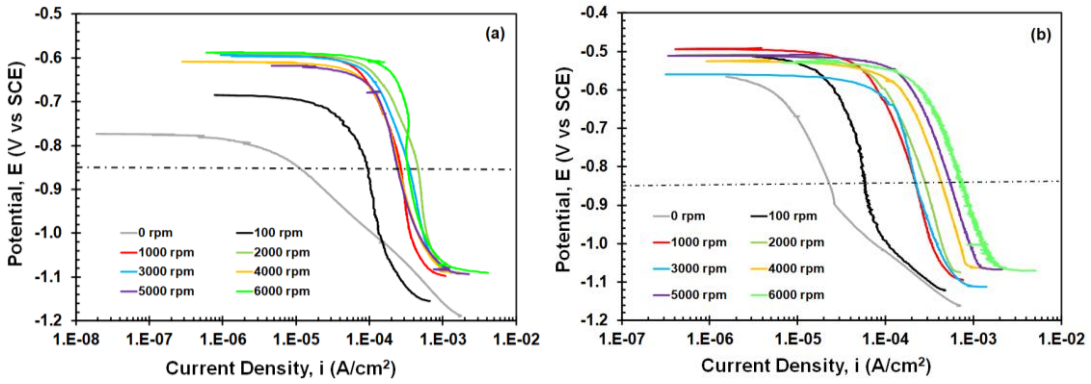

Figure 6. Cathodic polarization curves of X100 steel immersed in NACE brine at different rotation speed. a) Without corrosion inhibitor and b) with corrosion inhibitor. [55]

On the other hand, under turbulent flow conditions, is not observed a contribution of charge transfer processes, because a mass transfer process limited de cathodic reaction and a well-defined a limiting current density of oxygen ($i_{lim,O2}$) is observed. This behavior is attributed to the turbulent flow existing in the medium and with that condition, the diffusion of the O_2 toward to metallic surface was accelerated provoking with this fact the increment in the oxygen reduction (reduction reaction) and, consequently the oxidation reaction was accelerated. [54]

However, there exists a special behavior at 3000 rpm where there is not increased in the current density, in fact, the opposite behavior happened, the $i_{lim,O2}$ decreased. The behavior observed in the $i_{lim,O2}$ at 3000 rpm is reported in research works carried out by Galván-Martínez [45] and Lopez-Celvera [46], where the decrease of the $i_{lim,O2}$ was also observed.

In a general way, it can be observed that at all rotation speed tested, a limiting current density section can be identified. This $i_{lim,O2}$ is shifted to higher current density values as the rotation speed of the RCE is increased. These observations indicate that the cathodic kinetics may be described by a diffusion-controlled process. [56] In addition, it is important to point out that the inhibitor effects just can be observed to at the RS from 100 to 3000 rpm, after these RS, this effect trend to decrease

3.4.1. Mass transfer by Eisenberg empirical equation

In order to analyze the turbulent flow in a corrosion process, there exists an empirical expression that involves two fundamental aspects: the electrochemistry of the corrosion process and the hydrodynamics (rotation speed) of the working electrode in a RCE, this for a system influenced by the mass transfer processes. This expression is the Eisenberg Equation [57-61], which is shown in the equation 1.

$$i_{lim_i} = 0.079nFC_{b,i}d_{RCE}^{-0.3}\nu^{-0.334}D_i^{0.664}\,U_{RCE}^{0.7} \qquad (1)$$

Where *n* is the number of exchanged electrons in the electrochemical reaction, *F* is the Faraday constant, $C_{b,i}$ is the concentration of the electroactive species, D_{RCE} is the RCE diameter, *v* is the kinematic viscosity, D_i is the diffusion coefficient of electroactive species and U_{RCE} is Rotation speed.

Physicochemical properties of the NACE brine indicate that the pH is close to neutral (slightly basic) and additionally, the brine used was aerated; according to these two conditions, the main electroactive specie used in the cathodic analysis will be the oxygen. It is important to point out that the cathodic current density (i_{cat}) was determined experimentally from the cathodic polarization curves showed in figure 6. To obtain i_{cat} from each cathodic polarization curve, current density values were obtained at a defined potential, -0.85 V vs SCE [38], where it was compared with the theoretical current density of the O_2 ($i_{lim, O2}$) obtained from the Eisenberg equation and the i_{corr} obtained by the APC, such as it is shown in Figure 7.

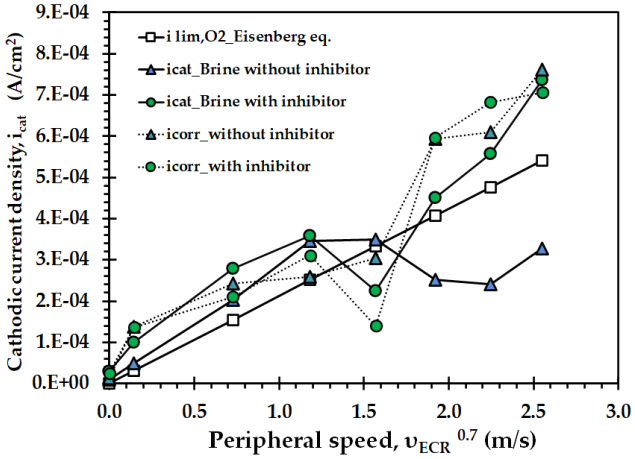

Figure 7. Experimental cathodic current density i_{cat} of the X100 steel immersed in NACE brine with and without corrosion inhibitor and theoretical current density of the O_2 ($i_{lim, O2}$) obtained from Eisenberg equation.

Figure 7 shows that the i_{cat} of the steel without inhibitor increases with respect to the peripheral speed of the cylinder, however, it only happens up to 2000 rpm (equivalent to 1.2 m/s) with a value of $4.5x10^{-4}$ A/cm^2, after this peripheral speed, the i_{cat} decreased to finally at 6000 rpm (3.81 m/s) the i_{cat} value incremented to $3.28x10^{-4}$ A/cm^2.

In case of the steel with corrosion inhibitor, the increment of the i_{cat} values were directly proportional to the peripheral speed, except for the one obtained at 1.5 m/s (3000 rpm), where the i_{cat} decreased. [44,45] This behavior agrees with the corrosion phenomenon previously described in the cathodic polarization curves, it is, the corrosion phenomenon is limited by a oxygen transport from the bulk fluid to metallic surface, and the turbulent flow accelerated the oxygen diffusion provoking that the reduction reaction was accelerated and, consequently the oxidation reaction. [54]

The behavior observed in the i_{cat} corroborated the behavior observed in the cathodic polarization curves, where the corrosion inhibitor just has a protective effect to 2000 rpm or 1.9 m/s. This behavior is attributed to the chaotic environment where the high Re (consequently high turbulence) can broke the adsorbed protector film formed by the corrosion products film and products formed by the inhibitor

It is important to point out that there exists a good correlation between the i_{cat} obtained in the cathodic curves in both systems, however, the better correlation between the i_{cat} of the steel and the theoretical $i_{lim,O2}$ was observed in the curve corresponding to i_{cat} of the steel immersed in NACE brine with inhibitor. Therefore, this behavior also corroborate that the corrosion system is under the influence of O_2 diffusion from the bulk fluid to the metallic surface. [38] According to this fact, the mass transfer process limited the cathodic corrosion process of the steel immersed in NACE brine with and without corrosion inhibitor under turbulent flow conditions.

It is important to point out that the i_{corr} values obtained by the APC also have a good correlation with the theorical $i_{lim,O2}$ obtained by Eisenberg empirical equation. This fact is attributed to the electrochemical reaction (anodic and cathodic reactions) trend to equilibrium, it is, the sum of the anodic current value and cathodic current value trend to zero in the E_{corr}.

3.4.2. Corrosion process at turbulent flow conditions by dimensionless numbers analysis

Figure 5 shows the Sherwood number (mass transfer coefficient by dimensionless number) and the oxygen mass transfer coefficient K_{O2} for the steel immersed in NACE brine with and without corrosion inhibitor under hydrodynamic conditions. In this Sh number is possible to correlate the Reynolds number (Re) and the Schmidt number (Sc) and so relate the physicochemical properties of the fluid, the electroactive species present in the medium and the hydrodynamics of the fluid [62-63], as shown in equation 3:

$$Sh = 0.0791 Re^{0.7} Sc^{0.356} \quad (3)$$

Where Sc is the Schmidt Number. This Sc number define the properties of the mass transport in a fluid of a specific specie. Sc is calculated according to equation 4.

$$Sc_i = \frac{\nu}{D_i} \quad (4)$$

Where a mass transfer process influenced by a diffusion of an "i" specie, the limiting current density ($i_{lim,i}$) and the mass transfer coefficient can relate according to follow expression:

$$k_i = \frac{i_{lim,i}}{nFC_{bi}} \quad (5)$$

Figure 8 was observed that as the Re number increased, the Sh number value also increased corroborating that the oxygen transfer from the bulk to the metallic surface is a hydrodynamic function of the system. In addition, in figure 8 is observe, in a second axis, the oxygen mass transfer coefficient (K_{O2}) as a function of the Re number.

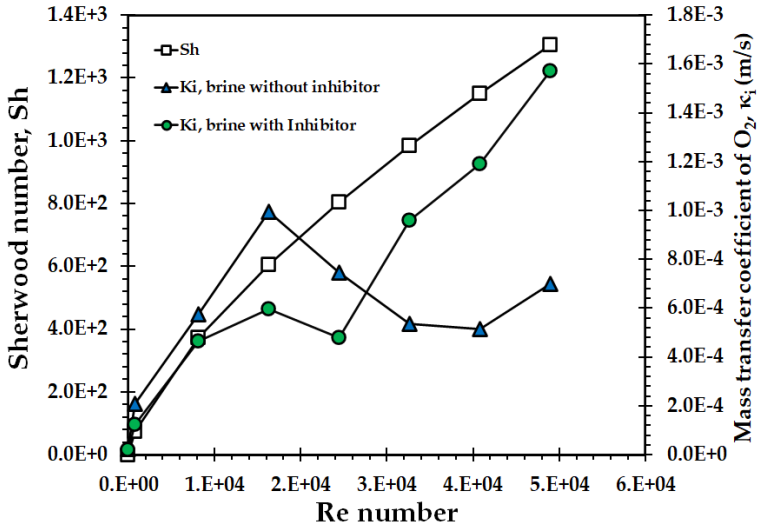

Figure 8. Oxygen mass transfer coefficient and Sherwood dimensionless number vs peripheral speed of the RCE. X100 steel immersed in NACE brine with and without corrosion inhibitor.

It can be observed that, as the Re number increased, the mass transfer coefficient also increased, this fact is correlated with the behavior of the i_{cat} curves presented in Figure 7. [64] It is because in order to calculate K_{O2}, the experimental cathodic current density is used, for that reason, i_{cat} and K_{O2} curves present a similar behavior. In case of brine with inhibitor, the K_{O2} values were obtained from $2.00x10^{-04}$ to $1.60x10^{-03}$ m/s, while in brine without inhibitor the K_{O2} value decreased to $7.00x10^{-04}$ m/s. In a general way, the K_{O2} values increased as the Re number also increased, except the values obtained at 24473.5 (3000 rpm).

It is important to point out that the measure of the interaction between metallic surface and fluid is important in the corrosion studies at turbulent flow conditions. The measures of these interactions are called wall shear stress ($\tau_{\omega,RCE}$) [65] The expression used in the calculation of $\tau_{\omega,RCE}$ was: [65-68]:

$$\tau_{w,RCE} = 0.079 Re_{RCE}^{-0.3} \rho U_{RCE}^{2} \qquad (6)$$

The Sh number and cathodic corrosion current density (i_{cat}) versus the wall shear stress of the RCE are shown in Figure 8. It is important to remember that the Eisenberg Equation is an empirical expression that analysis the hydrodynamics conditions for a corrosion process when it is influenced by a mass transfer process. [69]

Figure 8 (a) shows the behavior of the i_{cat} and the $\tau_{\omega,RCE}$ as a function of the Re number. This figure shows that as the Re number increased, the $\tau_{\omega,RCE}$ generated between the fluid movement and the metallic surface also increased provoking the rupture of the films formed on metallic surface. This fact can be corroborated with the i_{cat} behavior because it also increased generating the increment in the metal degradation. It is important to point out that the i_{cat} decreased in the Re numbers range of the 24473 to 32631, but after these values, the i_{cat} increased again. On the other hand, figure 8 (b) show that both variables, Sh number and i_{cat} can be influenced by the wall shear stress, it is because as the $\tau_{\omega,RCE}$ values increased, the mass transfer of the oxygen also increased provoking the acceleration of the cathodic

reaction and incrementing the corrosion speed. In case of i_{cat}, the wall shear stress can break or reduce the layer thickness (corrosion products plus products generate by the inhibitor) adsorbed on metallic surface and generate the increment of the active surface where the charge transfer can happen.

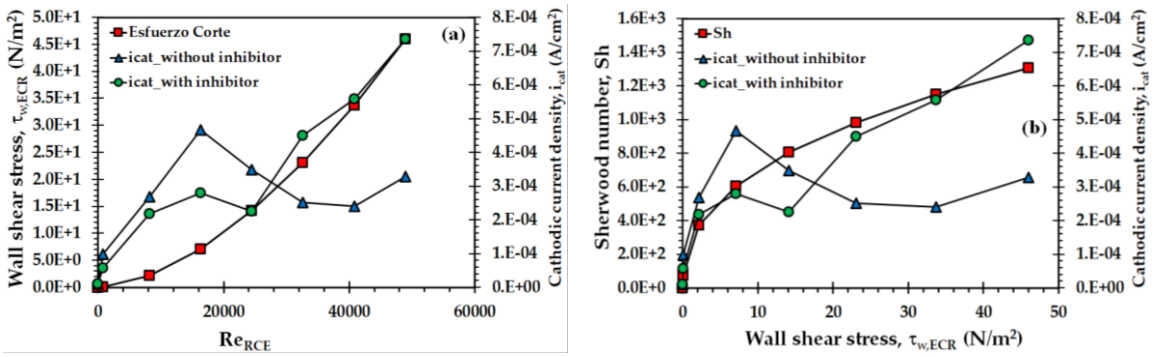

Figure 8. Wall shear stress and i_{cat} versus Re number (a) and i_{cat} and Sh dimensionless number versus wall shear stress (b). X100 steel immersed in NACE brine with and without corrosion inhibitor.

In a general way, it is possible to point out that in a cathodic corrosion process under turbulent flow conditions, the corrosion speed is dependent to the mass transfer of the electroactive specie from de bulk fluid to metallic surface, and the wall shear stress generated between the fluid movement and the metallic surface.

4. CONCLUSIONS

According to the analysis of the anodic and cathodic kinetics of X100 steel immersed in NACE brine with and without corrosion inhibitor under different rotation speed is possible to conclude that the corrosion potential got the stable state at 4000 rpm approximately. This behavior was presented for both conditions (brine with and without inhibitor), except to the E_{corr} at 3000 rpm in brine with inhibitor.

In the cathodic polarization curves, the steel without corrosion inhibitor showed a charge transfer process at static conditions but as the rotational speed of the RCE increased, this process was influenced by a mass transfer process. On the other hand, the corrosion of X100 steel immersed in NACE brine with corrosion inhibitor, it was limited by a mass transfer process, this is, the oxygen transfer from the fluid bulk to the metallic surface. In a general way is possible to point out that at turbulent flow conditions, the corrosion phenomenon is limited by a diffusion process. This behavior agrees with theoretical current density of the O_2 obtained by Eisenberg equation.

In addition, the theoretical $i_{limi,O2}$ does apply to the corrosion phenomenon limited by charge transfer process. This behavior can be corroborated with the i_{corr} obtained by APC, where the values of i_{corr} at both conditions have good agreement with the theorical Eisenberg equation. It is important to point out that all anodic Tafel slopes have values corresponding to charge transfer process indicating

with this fact that although the i_{corr} obtained by APC is flow dependent, the corrosion process in the anodic reaction is limited by an activational or charge transfer process.

It is important to point out that as the rotating speed (or peripheral speed) incremented, the coefficient of oxygen mass transfer and the Sherwood number also increased in direct way indicating with this fact that the cathodic reaction (oxygen reduction) was accelerated. The wall shear stress had a direct influence in the corrosion phenomenon because as the $\tau_{w,RCE}$ increased, k_{O2} (consequently i_{cat}) and i_{corr} also increased.

ACKNOWLEDGMENTS
The authors express their gratitude to National Council for Science and Technology (CONACYT), the Foundry Laboratory from Institute of Metallurgy and Materials Research of the Michoacana University and the Doctorate Program of Materials and Nanoscience of MICRONA Center of the Veracruzana University for the financial and technical support to C. Campechano-Lira for the realization of this research.

CONFLICTS OF INTEREST
The authors declare no conflict of interest.

References

1. J. C. Villalobos, A. Del-Pozo, B. Campillo, J, Mayen and S. Serna, *Metals*, 8 (2018) 351.
2. Y. D Han, R. Z Wang, H. Y. Jing, L. Zhao, L. Y. Xu, P. Xin, *Int. J. Hydrog. Energy Energy*, 45 (2020) 20094
3. I, Tamura, H. Sekine, and T. Tanaka. Thermomechanical Processing of High Strength Low Alloy Steels, Butterworth-Heinemann (2013), Bodmin, Cornwall. UK
4. Y. Yarai, H. Nagayama, J. Nakamura, M. Hamada, K, Kondo, H. Hirata and N. H. T. Murase, *Nippon Steel & Sumitomo Metal Technical Report*, 107, 295-462 (2015).
5. M. Montoya-Rangel, N. Garza-Montes de Oca, C. Gaona-Tiburcio, R. Colás, J. Cabral-Miramontes, D. Nieves-Mendoza, E. Maldonado-Bandala, J. Chacón-Nava and F. Almeraya-Calderón, *Metals*, 10 (2020) 1232.
6. J. Xu, R. D. K. Misra, B. Guo, Z., Jia and L. Zheng, *Mater. Sci. Eng., A*, 574 (2013) 94.
7. M. A. Islam, Z. Farhat. *Wear*, 376 (2017) 533.
8. Y. Xu and M. Y. Tan, M. Y. *Corros. Sci*., 151 (2019) 163.
9. W. Li, B.F.M. Pots, X. Zhong, S. Nesic, *Corros. Sci*., 126 (2017) 208.
10. T. Y. Jin, Y. F. Cheng. *Corros. Sci.*, 53 (2011) 850.
11. V. Javaheri, N. Khodaie, A. Kaijalainen, D. Porter, *Mater. Charact.*, 142, (2108) 295.
12. L. Y. Xu, Y. F. Cheng, *Corros. Sci.*, 59, (2012) 103.
13. E. Mahdi, A. Rauf, E. O. Eltai, *Corros. Sci.*, 83 (2014) 48.
14. A. B. Radwan, M. H. Sliem, P. C. Okonkwo, M. F. Shibl and A. M. Abdullah, *J. Mol. Liq.*, 236, (2017) 220.
15. H. M. Flower, High Performance Materials in Aerospace - Structural steels, (1995) Pondicherry, India.
16. D. T. Llewellyn and R. C Hudd, Engineering Steels in Steels: Metallurgy and Applications, Elsevier, Butterworth-Heinemann, Oxford, UK .
17. G. Cesari, F. W. Panella and A. Pirinu, A. *Eng. Fail. Anal.*, 116 (2020) 104745.
18. Y. Cheng, Y. Bai, Y., Li, Z., & Liu, J. *Anti-Corros. Methods Mater*. 66 (2019) 671.
19. J. Aguirre, M. Walczak, M. Rohwerder, *Wear*, 438 (2019) 203053.

20. B. A. F Santos, R. C. Souza, M. E. D. Serenario, M. C. Gonçalves, E. M. Júnior, T. A. Simões, A. H. S. Bueno , *J. Nat. Gas Sci. Eng.* 80 (2020) 103405.
21. M. Lara-Banda, C. Gaona-Tiburcio, P. Zambrano-Robledo, M. Delgado-E, J. A. Cabral-Miramontes, D. Nieves-Mendoza, E. Maldonado-Bandala, F. Estupiñan-López, J. G. Chacón-Nava, F. Almeraya-Calderón, *Materials* 13, (2020) 2836.
22. J. M. Jáquez-Muñoz, C. Gaona-Tiburcio, J. Cabral-Miramontes, D. Nieves-Mendoza, E. Maldonado-Bandala, J. Olguín-Coca, L. D. López-Léon, J. P. Flores-De los Rios, F. Almeraya-Calderón, *Metals* 11 (2021) 105.
23. H.-Y. Ha, J.-Y. Kang, J. Yang, C. D.Yim, B. S. You, *Corros Sci.*, 75 (2013) 426.
24. F. F. Eliyan and A. Alfantazi, *Corros. Sci*., 74 (2013) 297.
25. V. Kain, *Procedia Eng.*, 86 (2014) 576.
26. M. Finšgar and J. Jackson. *Corros. Sci*., 86 (2014) 17.
27. J. Liao, W. Zhang, J. Zhang, Z. Yang, F. Xu, Q. Peng, Z. Li, S. Qiu, *Corros Sci.*, 190 (2021) 109635.
28. S. Papavinasam, Evaluation and Selection of Corrosion Inhibitors, John Wiley & Son, Inc, (2000) Canada.
29. F.C. Walsh, G. Kear, A.H. Nahle, J.A. Wharton, L.F. Arenas, *Corros. Sci*, 123, (2017)1.
30. A.N. Colli, J.M. Bisang, *Int. J. Heat Mass Transfer*, 137 (2019) 835.
31. H. K. Rashid, A. A. Khadom, H. B. Mahood, A. N. Campbell. *Case Studies in Chemical and Environmental Engineering* 2 (2020) 1.
32. S. Arzola-Peralta, J. Mendoza-Flores, R. Duran-Romero, J. Genesca, *Corros. Eng. Sci. Technol.* 41 (2006) 321.
33. R.B. Bird, W.E. Stewart and E.N. Lightfoot, Fenómenos de transporte, Limusa Wiley (2006) México.
34. D.R. Gabe, *J. Appl. Electrochem.*, 4 (1974) 91
35. D.R. Gabe, F.C. Walsh, *J. Appl. Electrochem.*, 13 (1983) 3.
36. D.C. Silverman, *Corrosion*, 40 (1984) 220.
37. D.C. Silverman, Rotating Cylinder Electrode - An Approach For Predicting Velocity Sensitive Corrosion, Corrosion/90, NACE, Houston TX, 1990
38. R. Galván-Martínez, R. Orozco-Cruz, J. Mendoza-Flores, A. Contreras, J. Genesca, Hydrodynamics - Optimizing Methods and Tools, Study of the Mass Transport on Corrosion of Low Carbon Steel immersed in Sour Solution under Turbulent Flow Conditions, H. E. Schulz, A. L. Andrade Simões & R. Jahara Lobosco (eds), Intech Publishers, (2011) Croatia.
39. K. Oppenlaender, K. Stork and K. Barthold, Patent and Trademark Office, 4, ,114. Washington, DC: U.S. (1985).
40. R. Tyagi, V. K. Tyagi and S. K. Pandey, *J. Oleo Sci*., 56, (2007) 211.
41. NACE 1D182-2017-SG, Wheel Test Method Used for Evaluation of Film-Persistent Corrosion Inhibitors for Oilfield Applications, NACE International, Houston, Texas, (2017).
42. I. A. Aiad, A. A. Hafiz, M. Y. El-Awady and A. O. Habib, *J. Surfactants Deterg.*, 13 (2010) 247.
43. J. R. Welty, C. E. Wicks & R. E. Wilson, Fundamentos de Transferencia de Momento, Calor y Masa, (1994) Ed. LIMUSA - NORIEGA EDITORES, México.
44. E. Barmatov, T. Hughes, M. Nagl, *Corr. Sci*., 92, (2015) 85.
45. R. Galvan-Martinez, J. J. Ruíz-Martinez, R. Orozco-Cruz, M.A. Hernandez-Perez, A. Contreras, *ECS Transactions*, 94 (2019) 117.
46. S.A. López-Celvera, R. Orozco-Cruz, M.A. Baltazar, A. Contreras, R. Galván-Martínez, *ECS Transactions*, 84 (2018) 97
47. M. E. Olvera-Martínez, J. Mendoza-Flores. J. Genesca, in Efecto del Flujo Turbulento sobre el proceso de Corrosión por CO_2 y la Determinación de la Eficiencia de Inhibidores Corrosión, B. Valdez-Salas & M. Schorr Wiener (Eds.), pp.103-129, OmniaScience, (2016) Barcelona, España.
48. M. E. Olvera-Martínez, J. Mendoza-Flores, J. Genesca, *J. Loss Prev. Process Ind*., 35 (2015)19.

49. I. B. Onyeachu, I. B. Obot, A. Y. Adesina, *Corros. Sci*,, 168 (2020) 108589.
50. R.C. Barik, J.A. Wharton, RJK Wood, K.R. Stokes, Further studies into the flow corrosion cathodic mass transfer kinetics of copper and nickel-aluminium bronze wall-jet electrodes, Corrosion Science 170 (2020) 108660.
51. R. G. Kelly, J. R. Scully, D. W. Shoesmith, R. G. Buchheit, Electrochemical Techniques in Corrosion Science and Engineering, Tayleo and Francis, (2002), .Fl., United States of America.
52. Y. Meas, J. Uruchurtu, A. Martínez, F. J. Rodriguez, et-al, Técnicas Electroquímicas Para El Control y Estudio de La Corrosión, Ed. Juan Genescá Llongueras, UNAM, (2002) México
53. E. Barmatov, H. Trevor, E. Dmitry, *Corros. Sci*,, 103 (2016) 196.
54. I. B. Obot, I. B. Onyeachu, S. A. Umoren, *Corros. Sci.*, 159 (2019) 108140.
55. R. Galván-Martínez, C. Campechano-Lira, A. Bedolla-Jacuinde, M. A. Hernández-Pérez, R. Orozco-Cruz, ECS Trans., 94 (2019) 101.
56. M. E. Olvera-Martínez, J. Mendoza-Flores, F. Javier Rodríguez-Gómez, R. Durán-Romero, J. Genesca, *Mater. Corr.* 69 (2018) 376.
57. Y. Zheng, J. Ning, B. Brown, and S. Nešić, *Corrosion*, 72 (2016) 1519.
58. D.C. Silverman, *Corrosion*, 59 (2003) 207.
59. M. Al-Khateeb, R. Barker, A. Neville, and H.M. Thompson, *Corrosion*, 74 (2018) 971.
60. J. Y. Hwang, K. S. Yang, D. H, Yoon, K. Bremhorst, *Int. J. Heat Fluid Flow*, 29 (2008) 1268.
61. E.P. Rivero, P. Granados, F.F. Rivera, M. Cruz, I. Gonzalez, *Chem. Eng. Sci.*, 65 (2010) 3042–3049.
62. J. Mendoza-Flores, Kinetic studies of CO_2 corrosion processes under turbulent flow, University of Manchester, England, 1997.
63. M. Rahmani and J.E. Strutt, Hydrodinamic Modeling of Corrosion of Carbon Steels and Cast Irons in Sulfuric Acid, p.31, Materials Technology Institute of the Chemical Process Industries, Inc (1992) Houston, TX, USA.
64. R. Galván-Martinez, Estudio de la influencia del flujo turbulento sobre la corrosión de un acero al carbono en medios acuosos que contienen H2S disueltos - amargos (2004), UNAM, México.
65. PINE Research, Study of Mass Transport Limited Corrosion with Rotating Cylinder Electrodes: An Overview of Theory and Practice, Document #: DRA10077, REV004, (2020) p. 1-10.
66. K. Denpo and H. Ogawa *Corrosion*, 49 (1993) 442.
67. K. D. Efird, E. J. Wright, J. A. Boros, T. G. Hailey, *Corrosion*, 49 (1993) 992.
68. B. V. Johnson, H. J. Choi and A. S. Green. Effects of Liquid Wall Shear Stress on CO_2 Corrosion of X52 Steel Simulated Oilfield Production Environments, Proceedings of Conferences of NACE-Corrosion, Paper 00573, Houston TX, USA, 1991.
69. M. Eisenberg, C. W Tobias, R. C. Wilke, *J. Electrochem.Soc.*, 101, 6, (1954) 306.